Clinical Cancer Research

The IGF2/IR/IGF1R Pathway in Tumor Cells and Myofibroblasts Mediates Resistance to EGFR Inhibition in Cholangiocarcinoma

Javier Vaquero[1,2,3], Cindy Lobe[1], Sylvana Tahraoui[1], Audrey Clapéron[1], Martine Mergey[1], Fatiha Merabtene[1], Dominique Wendum[1,4], Cédric Coulouarn[5], Chantal Housset[1,6], Christèle Desbois-Mouthon[1], Françoise Praz[1], and Laura Fouassier[1]

Abstract

Purpose: Cholangiocarcinoma (CCA) is a desmoplastic tumor of the biliary tree in which epidermal growth factor receptor (EGFR) is overexpressed and contributes to cancer progression. Although EGFR has been envisaged as a target for therapy, treatment with tyrosine kinase inhibitors (TKI) such as erlotinib did not provide therapeutic benefit in patients with CCA, emphasizing the need to investigate resistance mechanisms against EGFR inhibition.

Experimental Design: Resistant CCA cells to EGFR inhibition were obtained upon long-time exposure of cells with erlotinib. Cell signaling, viability, migration, and spheroid growth were determined *in vitro*, and tumor growth was evaluated in CCA xenograft models.

Results: Erlotinib-resistant CCA cells displayed metastasis-associated signatures that correlated with a marked change in cell plasticity associated with an epithelial–mesenchymal transition (EMT) and a cancer stem cell (CSC)–like phenotype. Resistant cells exhibited an upregulation of insulin receptor (IR) and insulin-like growth factor (IGF) 1 receptor (IGF1R), along with an increase in IGF2 expression. IR/IGF1R inhibition reduced EMT and CSC-like traits in resistant cells. *In vivo*, tumors developed from resistant CCA cells were larger and exhibited a more prominent stromal compartment, enriched in cancer-associated fibroblasts (CAF). Pharmacological coinhibition of EGFR and IR/IGF1R reduced tumor growth and stromal compartment in resistant tumors. Modeling of CCA-CAF crosstalk showed that IGF2 expressed by fibroblasts boosted IR/IGF1R signaling in resistant cells. Furthermore, IR/IGF1R signaling positively regulated fibroblast proliferation and activation.

Conclusions: To escape EGFR-TKI treatment, CCA tumor cells develop an adaptive mechanism by undergoing an IR/IGF1R-dependent phenotypic switch, involving a contribution of stromal cells. *Clin Cancer Res; 24(17); 4282–96. ©2018 AACR.*

Introduction

Cholangiocarcinoma (CCA) is a heterogeneous group of malignancies that displays a biliary epithelial cell phenotype (1). CCA can emerge at every point of the biliary tree, from the canals of Hering to the main bile duct, and thereby is classified as intrahepatic, perihilar, and distal CCA, which share some similarities but also present important intertumor and intratumor differences affecting the pathogenesis and outcome (1). The overall prognosis is very poor due to late clinical presentation and the ability of the tumor to develop chemoresistance (1, 2). Late diagnosis compromises the only effective therapeutic option, surgical resection, that is applicable in 20% of cases. Patients ineligible for surgery undergo a palliative treatment with a combination of gemcitabine and oxaliplatin (GEMOX; refs. 1, 3). In case of tumor progression after this first line of chemotherapy, there is no other treatment approved despite the identification of potential therapeutic targets.

Epidermal growth factor receptor (EGFR) plays a critical role in oncogenesis, which places it as one of the promising targets for therapeutic inhibition. Several studies, including ours, have shown the major contribution of EGFR to CCA cell proliferation, migration, and invasion (4–6). In addition, dysregulations of EGFR expression and signaling have been associated with tumor progression and poorer prognosis in CCA patients (7, 8). However, despite EGFR attractive position as a molecular target for therapy, several independent clinical trials have reported very poor responses in patients with CCA treated with different small tyrosine kinase inhibitors (TKI) and monoclonal antibodies designed to specifically target EGFR (9–14).

CCA is characterized by a dense desmoplastic stroma rich in alpha-smooth muscle actin (α-SMA)-positive cells known as cancer-associated fibroblasts (CAF), which have been shown to participate in cancer progression (15). In this context, CAFs are

[1]Sorbonne University, INSERM, Saint-Antoine Research Center (CRSA), Paris, France. [2]Fondation ARC, Villejuif, France. [3]LPP, CNRS, Ecole Polytech., Univ. Paris-Sud, Observatoire de Paris, Univ. Paris-Saclay, Sorbonne University, PSL Research University, Paris, France. [4]Assistance Publique-Hôpitaux de Paris, Saint-Antoine Hospital, Department of Pathology, Paris, France. [5]INSERM, INRA, Univ Rennes 1, Univ Bretagne Loire, Nutrition Metabolisms and Cancer (NuMeCan), Rennes, France. [6]Assistance Publique-Hôpitaux de Paris, Saint-Antoine Hospital, Hepatology Department, Paris, France.

Note: Supplementary data for this article are available at Clinical Cancer Research Online (http://clincancerres.aacrjournals.org/).

Corresponding Author: Laura Fouassier, INSERM, 27 rue de Chaligny, 75012 Paris, France. Phone: 33-6-98-77-40-01; E-mail: laura.fouassier@inserm.fr

doi: 10.1158/1078-0432.CCR-17-3725

Translational Relevance

Cholangiocarcinoma is a devastating desmoplastic cancer of the biliary tree, for which no targeted therapies have been approved so far. Although EGFR contributes to cholangiocarcinoma progression, treatment with EGFR inhibitors such as erlotinib has not provided therapeutic benefit in patients with cholangiocarcinoma. In this study, we identify cellular mechanisms by which cholangiocarcinoma cells escape EGFR inhibition. We demonstrate that treatment with an EGFR inhibitor leads to the development of adaptive mechanisms by cholangiocarcinoma cells that include a phenotypic switch toward mesenchymal and cancer stem cell phenotypes. This cell plasticity is driven by an upregulation of insulin-like growth factor 2 (IGF2)-dependent cell signaling, comprising the activation of insulin and IGF1 receptors (IR/IGF1R). In addition, we identify a cross-talk between cancer-associated fibroblasts (CAF) and tumor cells in response to EGFR inhibition that relays on IGF2-dependent cell signaling pathway. These novel insights provide rational basis for testing combined therapies against EGFR and IR/IGF1R.

known to influence the sensitivity of tumor cells to anti-EGFR treatment in other cancers (16, 17).

Unfortunately, little is known about the factors that limit anti-EGFR responsiveness in CCA. Besides genetic modifications, such as *KRAS* mutations that determine the lack of response to EGFR TKI, no other mechanisms that could explain the ability of CCA tumor cells to develop adaptive behavior to escape from anti-EGFR treatment have been investigated (14). Thus, in the present work, we aimed to decipher the molecular mechanisms underlying the nonresponse of CCA cells to prolonged EGFR inhibition.

Here, we show that, *in vitro*, the adaptive response of CCA cells to EGFR TKI erlotinib involved an upregulation of the insulin-like growth factor 2/insulin receptor/insulin-like growth factor 1 receptor (IGF2/IR/IGF1R) signaling axis, that in turn regulated CCA cell plasticity, including epithelial-to-mesenchymal transition (EMT) and cancer stem cell (CSC) characteristics. *In vivo*, in a subcutaneous xenograft model, erlotinib-resistant CCA cells showed increased tumorigenicity and their tumors exhibited a more prominent stromal compartment. In addition, *in vitro* modeling of CCA–CAF cross-talk showed that stromal fibroblasts expressed IGF2 that boosted IR/IGF1R signaling in CCA-resistant cells to protect them against the deleterious effect of erlotinib. Finally, we show a potential role for IR/IGF1R signaling in the regulation of fibroblast proliferation and activation. Thus, our data strongly suggest that the IGF axis is responsible for the adaptive response against erlotinib in CCA tumor cells with a contribution of stromal cells, providing a rationale for testing combined therapies against EGFR and IR/IGF1R.

Materials and Methods

Reagents

Erlotinib was purchased from LC Laboratories. BMS-536924 and linsitinib were obtained from Tocris and Selleckchem, respectively. IGF2 was purchased from PreproTech.

Cell culture and treatment

HuCC-T1 cells, derived from intrahepatic biliary tract, were kindly provided by Dr. G. Gores (Mayo Clinic, MN), EGI-1 cells, derived from extrahepatic biliary tract, were obtained from the German Collection of Microorganisms and Cell Cultures (DSMZ, Germany), and SK-ChA-1 and Mz-ChA-1 cells, derived from extrahepatic biliary tract, were obtained from Dr. A. Knuth (Zurich University, Switzerland). Cells were cultured in DMEM supplemented with 1 g/L glucose, 10 mmol/L HEPES, 10% fetal bovine serum (FBS), antibiotics (100 UI/mL penicillin and 100 μg/mL streptomycin), and antimycotic (0.25 μg/mL amphotericin B; Invitrogen). All cell lines expressed higher levels of EGFR than nonmalignant biliary epithelial cells (Supplementary Fig. S1A). CCA cells resistant to erlotinib were generated through a process of slowly escalating exposure to erlotinib (from 1 to 20 μmol/L). EGFR inhibition and reduced sensitivity to erlotinib of resistant cells were then determined (Supplementary Fig. S1B and S1C). Resistant cells were maintained in culture in the presence of the last well-tolerated concentration of erlotinib (i.e., 20 μmol/L for HuCC-T1 and EGI-1, and 5 μmol/L for SK-ChA-1 and Mz-ChA-1).

The cell lines hTERT-HSC and LX2, derived from human activated hepatic stellate cells, were kindly provided by Dr. L. Aoudjehane (ICAN, Paris, France). hTERT-HSC and LX2 were cultured in DMEM supplemented with 4.5 g/L glucose, antibiotics (100 UI/mL penicillin and 100 μg/mL streptomycin), antimycotic (0.25 μg/mL amphotericin B), and 10% FBS and 2% FBS, respectively.

Cell lines were routinely screened for the presence of mycoplasma and authenticated for polymorphic markers to prevent cross-contamination.

Conditioned media

hTERT-HSC cells were grown to confluence, washed twice with phosphate-buffered saline (PBS), and 0% FBS DMEM (supplemented as above) was added for 48 hours. Conditioned media were centrifuged to remove cell debris and stored at −80°C until use. 0% FBS DMEM was used as control.

Microarray hybridization, processing, and data analysis

RNA quality was verified in an Agilent Bioanalyzer and quantified with a Nanodrop 1000 (Thermo Scientific). Microarray experiments were performed on Illumina humanWG-6 BeadChip (Post-genomics platform P3S, Sorbonne Université, Paris, France). Data were quantile normalized using BeadStudio software. The working lists were created by filtering probes with detection P values <0.05 for all the chips. Each dataset was derived from three biologically independent replicate samples. Statistical analysis of microarray data was performed using R-based BRB-ArrayTools as previously described (18). Briefly, genes differentially expressed between control and erlotinib-resistant cell lines were identified by a two-sample univariate t test and a random variance model. Gene set enrichment analysis (GSEA) was performed by using the Java-tool developed at the Broad Institute (Cambridge, MA) and the C2 collection of curated gene sets as previously described (18).

Viability assay

Cells were plated in 96-well plates. Twenty-four hours later, the medium was replaced by fresh culture medium or hTERT-HSC–conditioned medium with or without the corresponding concentrations of TKI, IGF2, and/or IGF2-neutralizing

antibody. Cells were then incubated for 72 hours before determining the viability by the crystal violet method. Absorbance was quantified with a spectrophotometer (Tecan) at 595 nm.

RNA and reverse transcription-PCR

Total RNA extraction and RT-qPCR was performed as previously described (5). Primer sequences are provided in Supplementary Tables S1 and S2. Gene expression was normalized to GAPDH mRNA content for human genes and to Hprt mRNA content for mouse genes and was expressed relatively to the control condition of each experiment. The relative expression of each target gene was determined from replicate samples using the formula $2^{-\Delta\Delta Ct}$. Qualitative evaluation of IR isoforms expression was conducted by PCR analysis using primers for the flanking exons 10 and 12 (Supplementary Table S3) and analyzed on 2% agarose gels (19).

Immunoprecipitation and Western blot analysis

For immunoprecipitation, cells were harvested in a buffer containing NP-40 (1%) supplemented with 1 mmol/L orthovanadate and a protease inhibitor cocktail (Roche Diagnostics) and subjected to centrifugation for 15 minutes at 4°C at 13,000 $\times g$. For obtaining whole-cell lysates, cell cultures were lysed in RIPA buffer supplemented with 1 mmol/L orthovanadate and a cocktail of protease inhibitors. Proteins were quantified using a BCA kit (Pierce). Immunoprecipitation and Western blot analysis were performed as previously described (5). Primary antibodies are provided in Supplementary Table S4.

Phospho-receptor tyrosine kinase (RTK) screening assay

A Human Phospho-RTK Array Kit (Catalog Number ARY001; R&D Systems) was used to measure the relative level of tyrosine phosphorylation of 49 distinct RTK. Six hundred micrograms of proteins were used, and the array was handled according to the manufacturer's instructions.

Immunofluorescence

Immunofluorescence assays were performed as previously described (5). Primary antibodies are provided in Supplementary Table S4. Cells were observed with a SP2 confocal microscope (Leica).

Migration assay

Migration was analyzed in 6.5 mm Transwell with 8-μm pore polycarbonate membrane inserts (Corning). Cells were plated in 0% FBS culture medium in the upper chamber and 10% FBS culture medium as a chemoattractant and the corresponding combination of TKIs was added in the lower chamber. After 24 hours (HuCC-T1 and SK-ChA-1) or 72 hours (EGI-1 and Mz-ChA-1) of incubation, migrated cells on the lower surface were enumerated by microscopy following fixation by 4% paraformaldehyde for 15 minutes and nucleic acid staining with DAPI. Four random fields were counted per insert.

Flow cytometry analysis

For the determination of the CD44/CD24 phenotype, cells were washed with PBS, detached with accutase treatment, and resuspended in PBS supplemented with 0.5% BSA. Combinations of fluorochrome-conjugated monoclonal antibodies against human CD44 (FITC) and CD24 allophycocyanin (APC) were obtained from Beckman Coulter. Specific antibodies or the respective isotype controls were added to the cell suspension, as recommended by the manufacturer, and incubated at 4°C for 20 minutes. Cells were washed with PBS containing 0.5% BSA, centrifuged, and resuspended in PBS with 2% paraformaldehyde. The labeled cells were analyzed with a Gallios flow cytometer (Beckman-Coulter).

Sphere formation assay

Cells were plated in 6-well ultralow attachment plates (Greiner Bio One) in serum-free DMEM/F12 medium, supplemented with 100 mg/mL gentamycin (Sigma-Aldrich), B27 (Life Technologies), 20 ng/mL human epidermal growth factor (EGF, Life Technologies), 20 ng/mL human basic fibroblast growth factor (bFGF, Life Technologies), and 1% antibiotic–antimycotic solution (Life Technologies) at a density of 4×10^4 cells/well. Fresh sphere medium was added to plates after 4 days. After 7 days, spheres were counted on EVOS FL Cell Imaging System (Thermo Fisher Scientific). Results are expressed as a percentage of sphere-forming units (%SFU) from the total number of cells plated.

Xenograft tumor model

Animal experiments were performed in accordance with the French Animal Research Committee guidelines and all procedures were approved by a local ethic committee (No 01346.02). Cells (2×10^6) suspended in 60 μL of PBS were mixed with 60 μL of Matrigel growth factor reduced (Corning) and implanted subcutaneously into the flank of 5-week-old female NMRI-nu (nu/nu) mice (Envigo). Mice were housed under standard conditions in individually ventilated cages enriched with a nesting material and kept at 22°C on a 12-hour light/12-hour dark cycle with *ad libitum* access to food and tap water. Tumor growth was followed with a caliper, and tumor volume (V) was calculated as follows: xenograft volume $= xy^2/2$ where x is the longest and y, the shortest of two perpendicular diameters. In a first set of experiments, HuCC-T1 and EGI-1 control and erlotinib-treated cells were injected and the mice were maintained until tumors started to show signs of necrosis. In a second set of experiments, mice were injected with EGI-1 control and erlotinib-treated cells following the same protocol. When tumor volume reached approximately 300 mm^3, erlotinib (75 mg/kg; 5 days per week) alone or in combination with linsitinib (30 mg/kg; 5 days per week), both dissolved in DMSO 5% (vehicle) were administered by gavage for 15 days. During the 14 days of treatment animals showed no sign of toxicity, such as body weight loss (>15%), decreased food intake, or diarrhea.

The day of the sacrifice, a slice of the tumor was fixed in 10% formalin and embedded in paraffin, and the rest was cut in pieces and frozen in liquid nitrogen.

CCA specimens

Human intrahepatic CCA tumors ($n = 10$) were obtained from untreated patients who underwent liver resection in Saint-Antoine Hospital (AP-HP, Tumor bank HUEP, "Tumeur Est") in accordance with the French laws and regulations (CNIL, registration No. ckT0915543z). Characteristics of patients with CCA are provided in Supplementary Table S5. Adjacent non-tumor liver tissue of patients with CCA showed no significant fibrosis except in 1 patient who had chronic hepatitis B with few fibrous septa.

Immunohistochemical analysis

For immunohistochemistry, formalin-fixed paraffin-embedded tissue samples from mice xenografts or human CCA were cut in 4-μm sections and antigens were unmasked as indicated in Supplementary Table S4. Sections were incubated sequentially with H_2O_2 for 5 minutes, with Protein Block (Novolink Polymer Detection System; Novocastra Laboratories Ltd.) for 5 minutes, and with primary antibodies for 30 minutes (IGF1R overnight). Novolink Post Primary was applied for 15 minutes. Sections were finally washed and incubated with Novolink Polymer for 15 minutes. An automated staining system (Autostainer Plus, Dakocytomation) was used to perform immunostaining. The color was developed using amino-ethyl-carbazole (AEC peroxidase substrate kit; Vector Laboratories). Sections were counterstained with hematoxylin and mounted with glycergel (Dako).

Statistical analysis

Results were analyzed using the GraphPad Prism 5.0 statistical software. Data are shown as means ± standard error of the mean (SEM). For comparisons between two groups, parametric Student *t* test or nonparametric Mann–Whitney test were used. For comparisons between more than two groups, parametric one-way ANOVA test followed by a posteriori Bonferroni test was used.

Results

CCA cells undergo a phenotypic switch to escape EGFR inhibition

We first observed that long-term treatment of four CCA cell lines (HuCC-T1, EGI-1, SK-ChA-1, and Mz-ChA-1) with the EGFR TKI erlotinib caused a phenotypic switch with elongated fibroblast-like morphology and decreased cell–cell contacts while control cells appeared cuboidal and cobblestone-like (Fig. 1A). None of the CCA cell lines had mutations in the tyrosine kinase domain of *EGFR* gene before treatment and no secondary mutation was identified during treatment (data not shown). To identify adaptive mechanisms to EGFR inhibition in CCA cells, we performed a gene expression analysis at a pangenomic scale. GSEA revealed metastasis-associated signatures in CCA cells chronically treated with erlotinib that were different for each cell line (Fig. 1B). Together, the marked phenotypic switch between untreated and treated cells associated with the identification of metastasis signatures suggested that cells had undergone EMT, a biological process involved in metastasis.

To investigate this possibility, we examined by immunofluorescence the expression and localization of E-cadherin and β-catenin, two components of epithelial cell adherens junctions that are downregulated during EMT. Resistant CCA cells exhibited a downregulation of both proteins at the plasma membrane (Fig. 1C). The downregulation of E-cadherin protein was confirmed by Western blot and correlated with an increased protein expression of the EMT-inducing transcription factors (EMT-TF) ZEB1, SLUG, and SNAIL in resistant cells compared with control cells (Fig. 1D). No expression of ZEB2 or TWIST1/2 was found in any cell line (data not shown). Resistant cells also overexpressed mesenchymal markers among MMP1, MMP3, vimentin, S100A9, and fibronectin (Fig. 1E). Of note, the EMT-TF and mesenchymal markers upregulated in resistant cells were different depending on the cell line, as noticed for the metastasis-associated signatures (Fig. 1B and E). To evaluate if all these molecular changes were associated with differences in migratory function, we performed transwell chamber assays. This analysis showed a significant increase in the migratory capacities of HuCC-T1–, SK-ChA-1–, and Mz-ChA-1–resistant cells (Fig. 1F). Because in EGI-1–resistant cells we did not find differences compared with the controls, migratory function was measured by another approach. Time-lapse microscopy showed, indeed, an increase in EGI-1–resistant cell motility (Supplementary Fig. S2). Collectively, these data demonstrate that, despite the heterogeneity of the molecular markers modified in resistant cells, CCA cells develop a common adaptive mechanism in response to chronic EGFR inhibition by undergoing EMT.

CCA cells exhibit stemness features to escape EGFR inhibition

Increasing evidence suggests that EMT is associated with the acquisition of cancer stem cell (CSC)-like features (20), thereby conferring resistance to chemotherapies in cancer cells. Accordingly, GSEA showed signatures associated with stemness in all CCA cells resistant to EGFR inhibition (Supplementary Table S6). These signatures were confirmed by gene expression analysis of a panel of well-known CSC markers. Depending upon the cell line, ALDH isoforms, CD61, CD133, SOX9, or IGFBP7 were increased in resistant cells (Fig. 2A). Once more, the signatures and CSC markers modified in erlotinib-resistant cells were specific for each cell line. In addition, flow cytometry analysis on CD44/CD24 expression, two well-established CSC markers, showed in all CCA cell lines a shift from the $CD44^{high}/CD24^{high}$ to the $CD44^{high}/CD24^{low}$ quadrant, a signature ($CD44^{high}/CD24^{low}$) that is characteristic of a population with both EMT and CSC features (ref. 21; Fig. 2B). Sphere formation evaluation showed a higher number of spheres in HuCC-T1 and EGI-1–resistant cells, but not in SK-ChA-1 (Fig. 2C). The number of Mz-ChA-1 spheres was impossible to count due to giant sphere aggregates, which were bigger in erlotinib-resistant cells (Fig. 2C). These observations provide further evidence that CCA cells acquire certain attributes of CSC during adaptive mechanisms to EGFR inhibition.

IGF2/IR/IGF1R axis is upregulated in CCA cells resistant to EGFR inhibition

Activation of bypass signaling pathways is part of the adaptive mechanisms that determine nonresponse of tumor cells to anti-EGFR therapy in cancer (22, 23). To investigate whether activation of other RTK may compensate EGFR inhibition, we screened the total tyrosine phosphorylation of 49 RTK by antibody array. The common change observed between control and resistant cells in the four cell lines was a differential phosphorylation status of IR and/or IGF1R (Fig. 3A; Supplementary Fig. S3A), two related RTK with high structural and functional homologies. The increased phosphorylation of these RTK in resistant cells was confirmed by Western blot (Fig. 3B) without or after immunoprecipitation of individual receptors (Supplementary Fig. S3B). In addition, changes in IR/IGF1R tyrosine phosphorylation were accompanied by changes in the total expression (Fig. 3B), indicating that this mechanism may rely more on RTK upregulation than receptor activation. Increment in IR/IGF1R phosphorylation was accompanied by an increase in AKT phosphorylation in all resistant cell lines, compared with their control counterparts, while ERK signaling was also enhanced in EGI-1– and SK-ChA-1–resistant cells,

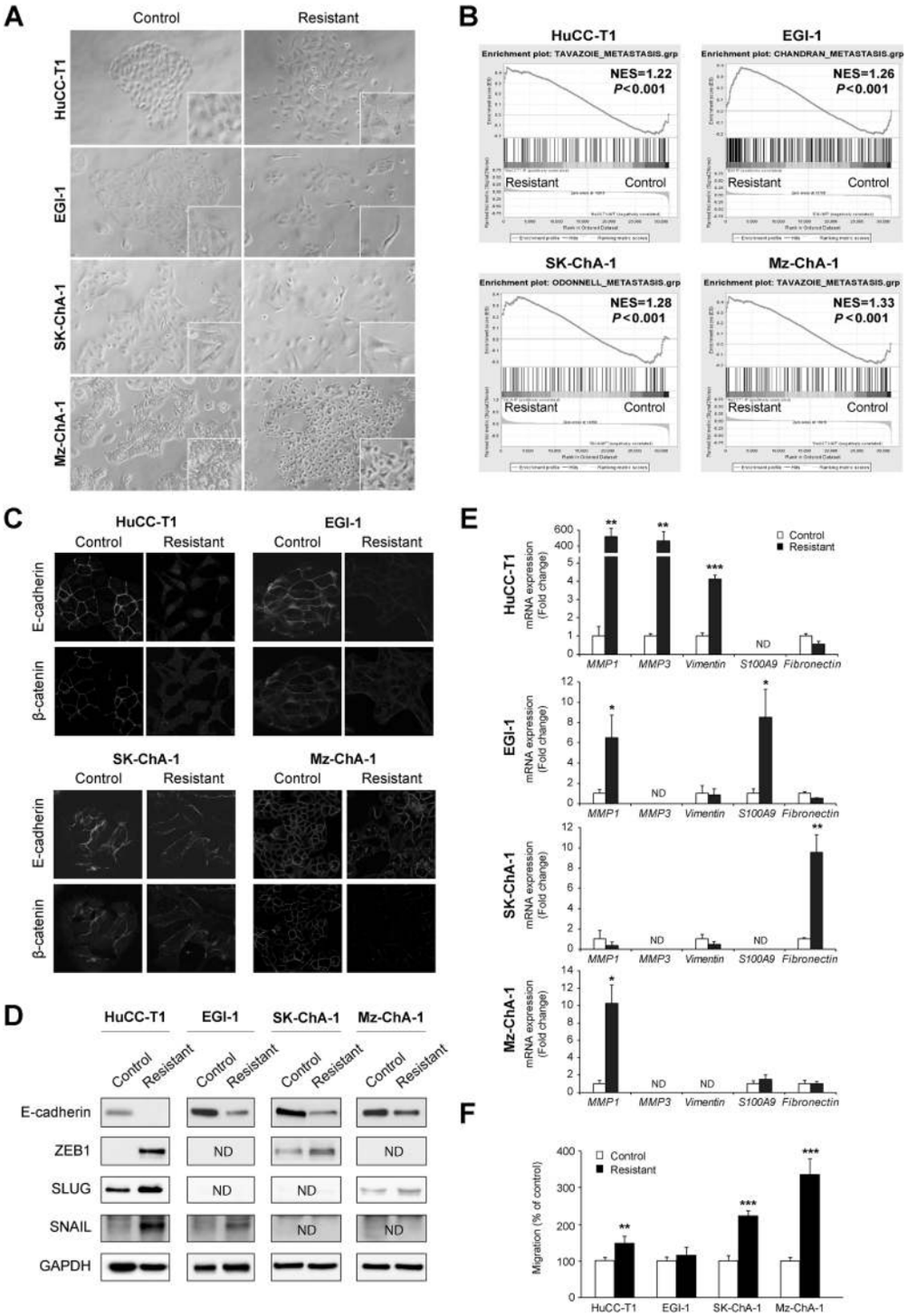

Figure 1.

CCA cells undergo a phenotypic change to evade EGFR inhibition. **A,** Representative phase-contrast photographs of control and erlotinib-resistant CCA cells showing a scattered phenotype. Magnification, ×10 and ×20 (insets). **B,** Enrichment of metastatic signatures in CCA cells resistant to EGFR inhibition as compared with control cells. Normalized enrichment scores (NES) were determined by GSEA algorithm ($P < 0.05$). **C,** Representative images of E-cadherin and β-catenin expression in CCA cells analyzed by immunofluorescence with a confocal microscope. Magnification, ×20. **D,** Representative images of Western blot analysis of E-cadherin and EMT-TF expressed by CCA cells. **E,** Changes in mRNA expression of mesenchymal markers in CCA cells analyzed by RT-qPCR. **F,** Cell migration toward a chemoattractant (serum) was measured by Transwell chamber assay. Values are expressed as means ± SEM from at least 3 independent cultures. *, $P < 0.05$; **, $P < 0.01$; ***, $P < 0.001$, as compared with control cells. ND, not detected.

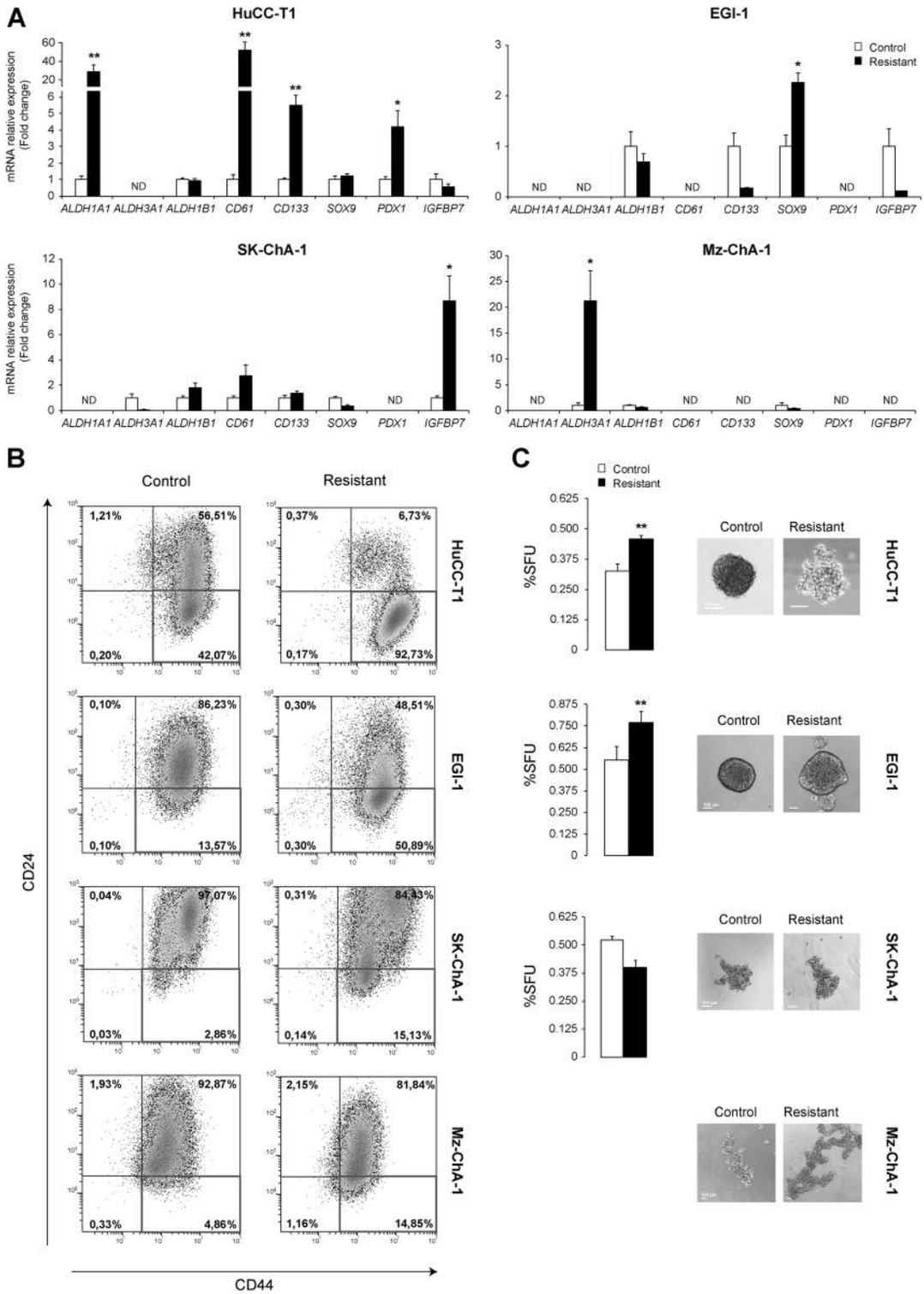

Figure 2.

CCA cells exhibit stemness features to escape EGFR inhibition. **A,** Changes in mRNA expression of CSC markers analyzed by RT-qPCR in control and CCA cells resistant to EGFR inhibition. **B,** CD44 and CD24 expression profile was assessed by flow cytometry using APC-conjugated anti-CD24 and FITC-conjugated anti-CD44 antibodies. Gates are based on the isotype controls. The numbers indicate the percentage of cells present in each quadrant. **C,** Sphere formation assay after 7 days in culture. Right, Representative pictures of control and resistant spheres. Scale, 100 μm. Values are expressed as means ± SEM from at least 3 independent cultures. *, $P < 0.05$; **, $P < 0.01$; ***, $P < 0.001$, as compared with control cells.

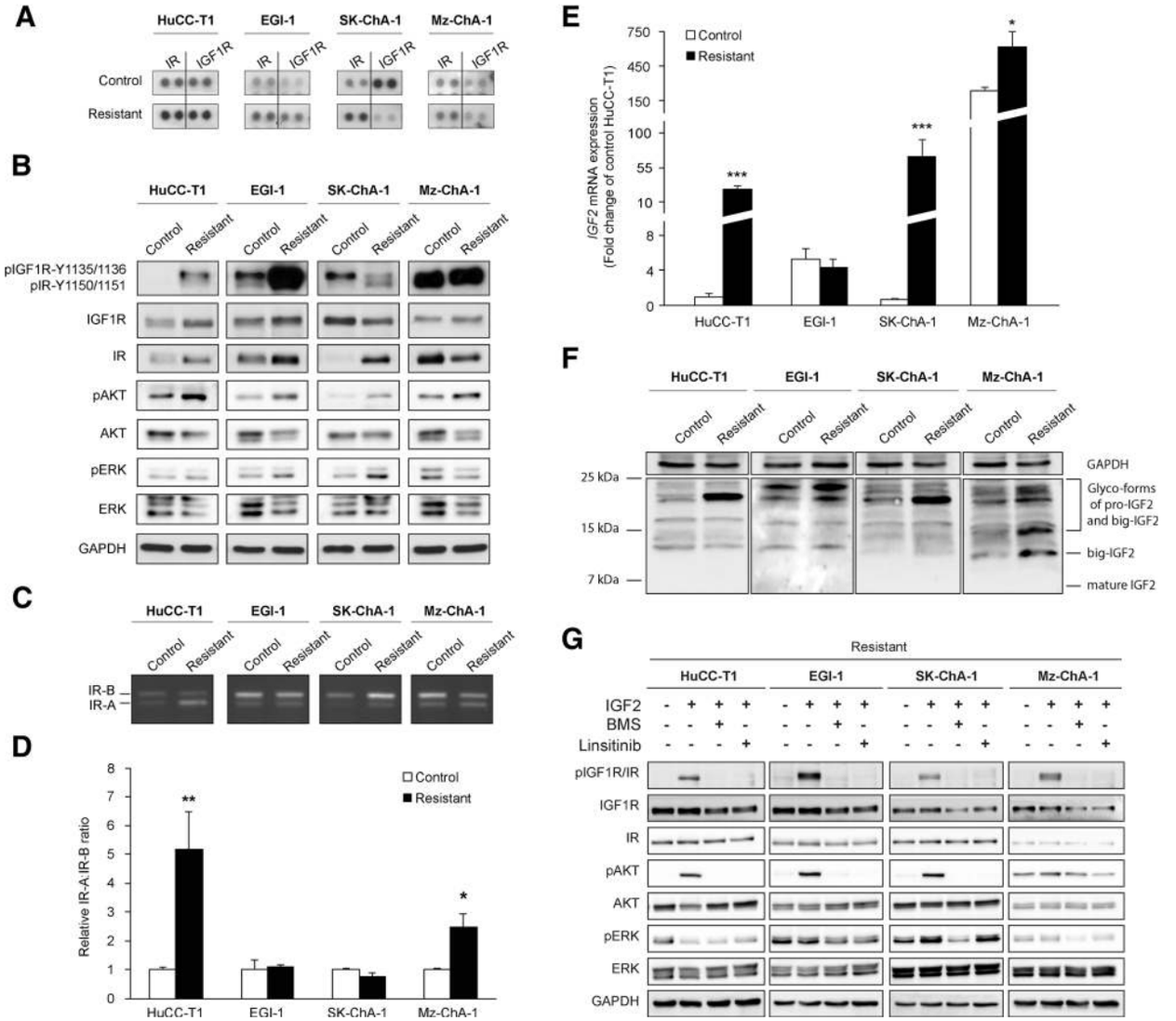

Figure 3.

The IGF2/IR/IGF1R axis is an escape route upregulated in CCA cells resistant to EGFR inhibition. **A,** Representative images of human phospho-RTK array of IR and IGF1R total tyrosine phosphorylation in control and resistant CCA cells. **B,** Representative images of Western blot analysis of IR, IGF1R, AKT, and ERK total expression and phosphorylation state in control and resistant CCA cells. **C** and **D,** Analysis of IR-A and IR-B mRNA expression by gel electrophoresis (**C**) and RT-qPCR (**D**). RT-qPCR results are represented as ratio of IR-A/IR-B (**D**). **E** and **F,** Analysis of IGF2 mRNA (**E**) and protein (**F**) expression in control and resistant CCA cells. **G,** Representative images of Western blot analysis of IR, IGF1R, AKT, and ERK total expression and phosphorylation state in control and resistant cells treated with IGF2 in the absence or presence of IR/IGF1R inhibitors, BMS536924 or linsitinib. Values are expressed as means ± SEM from at least 3 independent cultures. *, $P < 0.05$; **, $P < 0.01$; ***, $P < 0.001$, as compared with control cells.

unchanged in HuCC-T1–resistant cells, and decreased in Mz-ChA-1–resistant cells (Fig. 3B). Furthermore, IR is expressed as two isoforms, IR-A and IR-B, as a result of alternative splicing of exon 11. This structural feature confers specific functional properties to IR-A, such as higher affinity for IGF2 and oncogenic properties, compared with IR-B that is involved in the regulation of the metabolic functions (24). Both isoforms were detected in all cells, with an increase in IR-A:IR-B ratio in two resistant cell lines, HuCC-T1 and Mz-ChA-1 (Fig. 3C and D). The following step was to analyze the expression of IR/IGF1R ligands, IGF-1, IGF-2, and insulin. Only IGF2, the ligand that displays high affinity for both IR-A and IGF1R, was detectable at mRNA level, and its expression was enhanced in resistant cells compared with control cells (Fig. 3E). This increase was validated at the protein level by Western blot. While mature form of IGF2 was not detected, levels of the unprocessed forms, pro- and big- forms, of IGF2 were enhanced (Fig. 3F). It should be noted that unprocessed forms of IGF2 possess similar binding potential for IR/IGF1R as mature IGF2, but show impaired ternary complex formation, which allows them to exhibit higher bioavailability than the mature form (25). We did not identify epigenetic modifications such as methylation that could explain the increase in IGF2 production (data not shown). To further clarify the intracellular signaling elicited

by this ligand, resistant cells were starved and exposed to IGF2 in the absence or presence of two dual IR/IGF1R inhibitors, BMS536924 and linsitinib. As expected, IGF2 was able to activate IR/IGF1R, and this effect was followed by the activation of AKT in all resistant cell lines, while ERK was activated only in SK-ChA-1 resistant cells (Fig. 3G). Both BMS536924 and linsitinib exert their inhibitory effect over IR/IGF1R, which was followed by the inhibition of AKT signaling (Fig. 3G). Similar inhibitory effects of both BMS536924 and linsitinib were observed on IR/IGF1R and AKT phosphorylation, but not over ERK signaling, in conditions of culture activation (10% FBS; Supplementary Fig. S3C).

These results suggest that CCA resistance to erlotinib may depend on the upregulation of an alternative signaling pathway driven by IGF2/IR/IGF1R and by intracellular AKT signaling.

IR/IGF1R blockage regulates viability and cell plasticity of CCA cells resistant to EGFR inhibition

Given IR/IGF1R upregulation in CCA cells resistant to EGFR inhibition, we decided to test, on the parameters analyzed so far, the effect of the combination of erlotinib with BMS536924 and linsitinib. Both compounds were able to promote a strong decrease of resistant cell viability, but had little or no effect on control cells (Fig. 4A; Supplementary Fig. S4A). Consistently, IR/IGF1R TKI reduced EMT/CSC features, observed as a reduction of EMT-TFs expression, cell migration (Fig. 4B and C; Supplementary Fig. S4B and S4C) and sphere formation (Fig. 4D; Supplementary Fig. S4D) of resistant cell lines.

SiRNA knockdown of IR and IGF1R was performed to analyze their relative role in resistant cell lines. Western blot analysis showed a compensatory upregulatory effect of IR and IGF1R knocking down on each other, while dual siRNA knock down caused a profound downregulation of both receptors (Supplementary Fig. S5A). Functional tests showed (i) no evidence for a prominent role of one receptor over the other (Supplementary Fig. S5B–S5D) and that (ii) consistent with the effect of BMS536924 and linsitinib, dual downregulation of IR/IGF1R significantly reduced the viability (Supplementary Fig. S5B), migratory capacities (Supplementary Fig. S5C) and sphere formation (Supplementary Fig. S5D) of all resistant cell lines.

Altogether, these results indicate that during adaptation to EGFR inhibition, an alternative IGF2/IR/IGF1R pathway is upregulated, which contributes to regulate CCA cell plasticity.

In vivo, CCA cells resistant to EGFR inhibition show increased tumorigenic potential and higher tumor stroma content

To compare the tumorigenicity of control and resistant cells, subcutaneous xenografts in immunocompromised mice were performed with HuCC-T1 and EGI-1 cells. Subcutaneous injection of CCA cell lines demonstrated that resistant cells to erlotinib presented a higher tumorigenic potential compared with control cells (Supplementary Fig. S6A). When tumor histology was analyzed, it was evidenced that resistant tumors were less differentiated, with less glandular formation and the presence of marked cellular atypia (Supplementary Fig. S6B). In addition, resistant tumors displayed a higher stromal area than control tumors (Supplementary Fig. S6B). Because CCA stroma predominantly consists in CAFs, we evaluated the expression of well-established markers of fibroblast activation (α-SMA) and extracellular matrix production (collagens I and IV; ref. 26) and found an increment of these markers in resistant tumors compared with controls (Supplementary Fig. S6C).

IR/IGF1R blockage decreases tumor growth and stroma content of xenograft CCA tumors resistant to EGFR inhibition

To evaluate the effect of IR/IGF1R inhibition *in vivo*, EGI-1 cells were chosen because the tumors developed from these cells arose earlier in time with higher tumor burden than those from HuCCT-1 cells (Supplementary Fig. S6A). Thus, once tumors from EGI-1 control and resistance cells were well established and reached a similar volume (approximately 300 mm^3), mice were treated with erlotinib alone or in combination with linsitinib (the most efficient IR/IGF1R inhibitor in the *in vitro* experiments). As expected, erlotinib significantly inhibited growth of tumors developed from control cells without affecting resistant tumors (Fig. 5A–C). In contrast, combined treatment with erlotinib and linsitinib drastically reduced the growth of tumors developed from resistant cells to levels comparable with control tumors (Fig. 5A–C), indicating a role of IR/IGF1R blockage in overcoming tumor resistance to EGFR inhibition.

Based on the histologic analysis that showed a stronger desmoplastic reaction in tumors developed from resistant cells (Supplementary Fig. S6B and S6C), we analyzed the effect of IR/IGF1R inhibition on this aspect of tumor biology. To quantify the content of stroma, we performed immunohistochemistry (IHC) to detect α-SMA–positive cells (e.g., CAFs), and Picro-Sirius Red staining to evaluate the amount of collagen produced. An increased staining of α-SMA and collagens was found in resistant tumors compared with the controls, that was not modified upon erlotinib treatment but markedly reduced in animals that received combined treatment (Fig. 5D and E).

CAFs by producing IGF2 support IR/IGF1R signaling in CCA cells resistant to EGFR inhibition

Because stromal compartment was affected in tumors from mice under linsitinib treatment, we decided to look more closely at the IGF2/IR/IGF1R pathway in CAFs. We first analyzed by IHC the expression of IGF2 and IGF1R in mice tumors. IR expression was not analyzed due to unavailable antibodies for IHC. First, we confirmed that cancer cells from both control and resistant CCA tumors expressed IGF2 and IGF1R (Fig. 6A). Furthermore, we observed for the first time an expression of IGF2 and IGF1R in CAFs from xenograft CCA tumors (Fig. 6A). In human, because CCA samples from patients treated with erlotinib were not available, we performed an IHC analysis of IGF2 and IGF1R in intrahepatic CCA samples. This analysis showed IGF2 and IGF1R expression in CCA cells and CAFs, confirming our results from mice xenografts (Supplementary Fig. S7).

Because CAFs from CCA express IGF2, we next aimed at evaluating the contribution of CAFs in the activation of the IR/IGF1R pathway in resistant CCA cells. To model the cross-talk between CAFs and CCA cells, we performed *in vitro* experiments by using the established human liver–derived myofibroblast cell line hTERT-HSC (that showed higher IGF2 expression than LX2, Fig. 6B). Incubation of EGI-1 cells with conditioned medium from hTERT-HSC led to an increase in cell viability only in

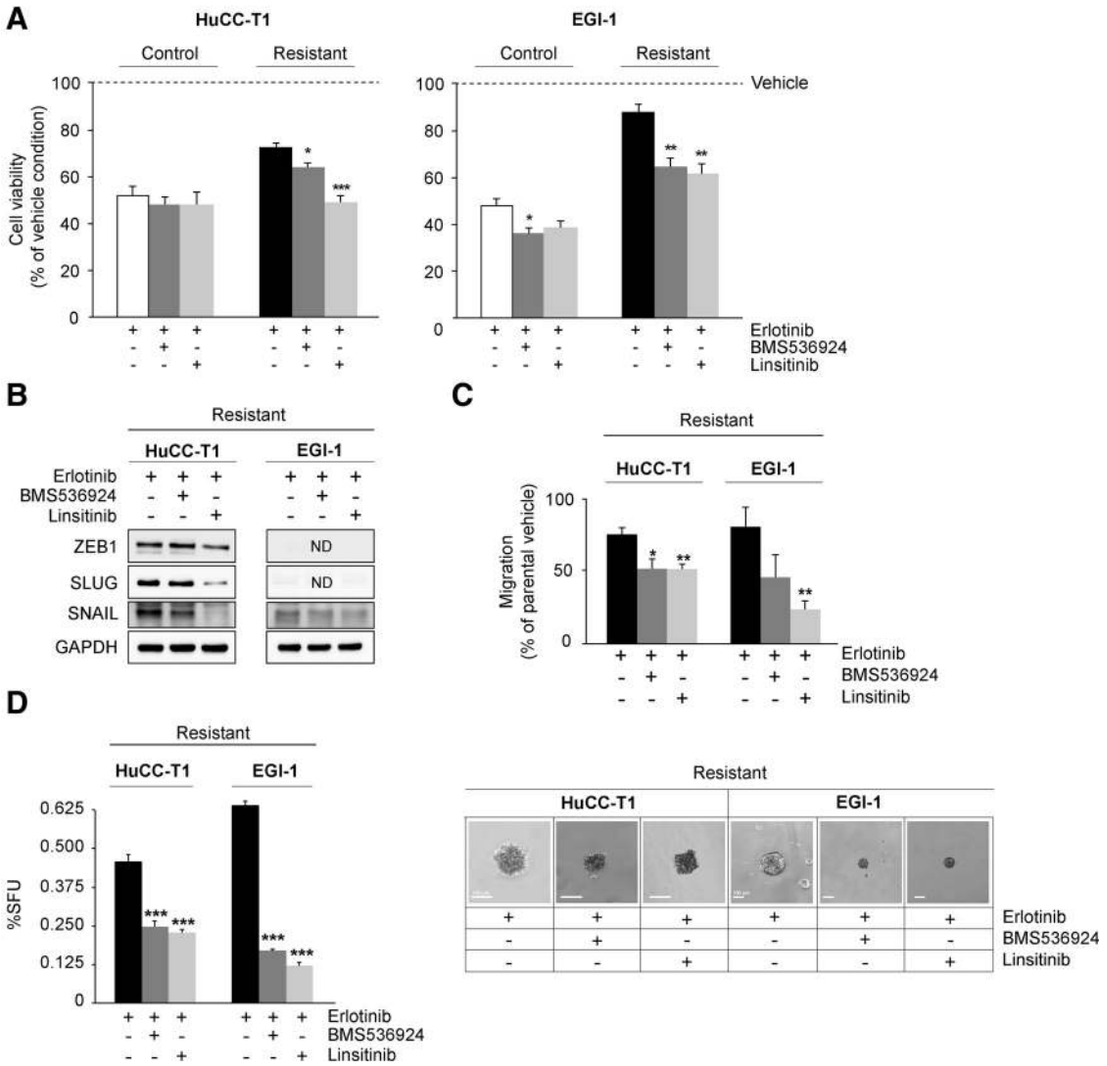

Figure 4.

IR/IGF1R blockage regulates viability and cell plasticity of CCA cells resistant to EGFR inhibition. **A,** Effect of IR/IGF1R inhibitors on the viability of control and resistant CCA cells. Cell viability was measured after incubation for 72 hours with erlotinib in the absence or presence of IR/IGF1R inhibitors, BMS536924 or linsitinib. The dotted line (vehicle) indicates the viability of the cells cultured in the absence of erlotinib. **B,** Representative images of Western blot analysis of the EMT-TF expressed by CCA cells after 48 hours under the indicated treatment. **C,** Cell migration toward a chemoattractant (serum) was measured by Transwell chamber assay. **D,** Sphere formation assay after 7 days under the indicated treatment. Right, Representative pictures of the largest spheres found for resistant cells under each treatment. Scale, 100 μm. In all cases, the concentrations of inhibitors were 20 μmol/L erlotinib, 1 μmol/L BMS536924, and 10 μmol/L linsitinib for HuCC-T1; and 20 μmol/L erlotinib, 0.5 μmol/L BMS536924, and 5 μmol/L linsitinib for EGI-1. Values are expressed as means ± SEM from at least 3 independent cultures. *, $P < 0.05$; **, $P < 0.01$; ***, $P < 0.001$, comparing cells treated with BMS536924 or linsitinib with untreated cells. ND, not detected.

resistant CCA cells, that was abolished by the addition of an IGF2-neutralizing antibody but not by an irrelevant IgG isotype (Fig. 6C). Accordingly, hTERT-HSC–conditioned medium was able to activate IR/IGF1R only in resistant cells (Fig. 6D). These results were validated in CCA cells upon IGF2 treatment alone or in combination with IGF2-neutralizing antibody. Stimulation with IGF2 promoted a small increase in control cell viability, while in resistant cells, it had a more pronounced effect (Fig. 6E). These results correlated again with a much higher activation of IR/IGF1R in resistant cells compared with controls upon IGF2 treatment (Fig. 6F). As expected, the addition of IGF2-neutralizing antibody abolished the effect of IGF2 (Fig. 6E), confirming the role of the IGF2/IR/IGF1R pathway in the resistance of CCA cells to EGFR inhibition.

Altogether, these results suggest the implication of a cross-talk between CAFs and tumor cells in the adaptive mechanism of CCA cells to EGFR inhibition through IGF2 originating from CAFs.

IR/IGF1R blockage downregulates hepatic myofibroblast proliferation, activation, and extracellular matrix synthesis

Given IGF2 production by the CCA cells and stromal myofibroblasts, we wondered if the IGF2/IR/IGF1R signaling

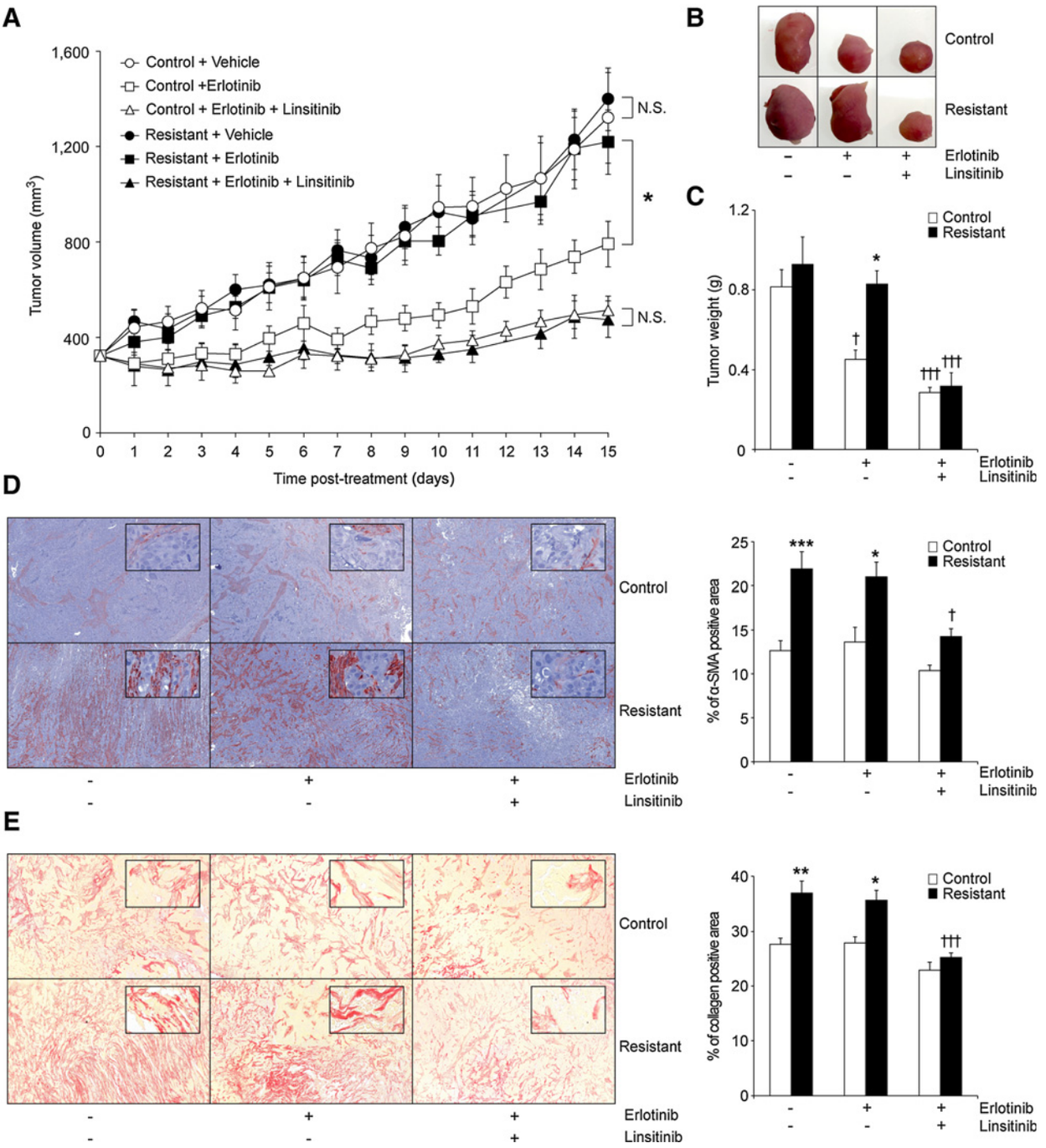

Figure 5.

IR/IGF1R blockage decreases tumor growth and stroma content of xenograft CCA tumors resistant to EGFR inhibition. **A,** Tumor volume of mice bearing control (white) or erlotinib-resistant (black) EGI-1 cells treated with vehicle (circles), erlotinib (squares, 75 mg/kg/day), or erlotinib/linsitinib (triangles, 75/30 mg/kg/day) for 15 days (5 days per week). **B,** Representative images of a tumor from each group at sacrifice. **C,** Tumor weight at sacrifice. **D** and **E,** Representative IHC of α-SMA (**D**) and Picro-Sirius Red (**E**) staining in mice CCA tumors and quantification of positive area with ImageJ (on the right). Magnification, ×5 and ×40 (insets). Values are expressed as means ± SEM. *, $P < 0.05$; **, $P < 0.01$; ***, $P < 0.001$, as compared resistant with control tumors. †, $P < 0.05$; ††, $P < 0.01$; †††, $P < 0.001$, as compared with untreated tumors of each group ($n = 7$).

pathway had a role in the latter cell type. Both hepatic myofibroblast cell lines, hTERT-HSC and LX2, expressed IR and IGF1R at the protein level, and both receptors were responsive to IGF2 (Fig. 7A). In these cells, IGF2 was able to promote proliferation (Fig. 7B). In addition, IR/IGF1R inhibition by linsitinib decreased cell viability in a dose-dependent manner

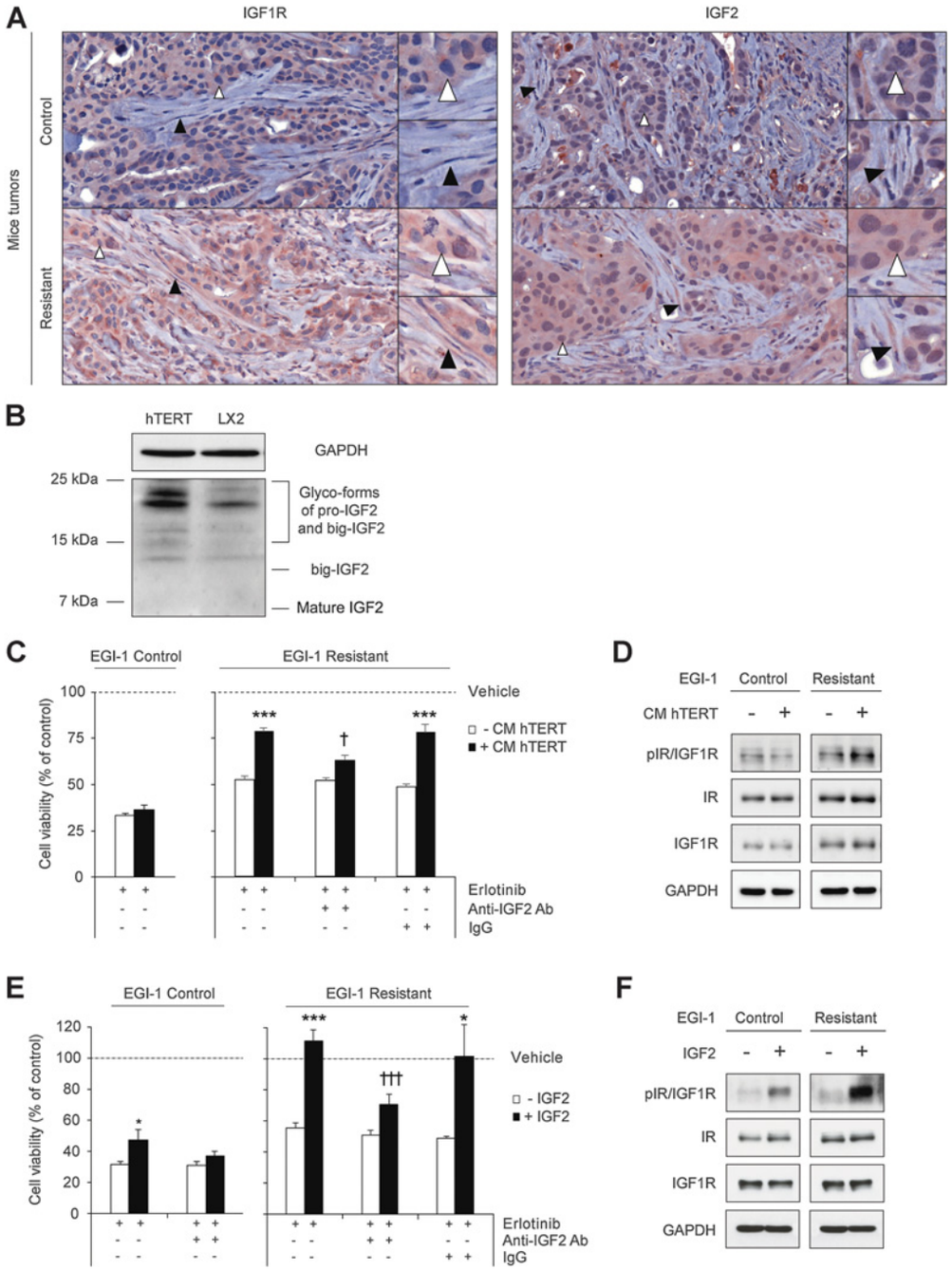

Figure 6.

CAFs support IR/IGF1R signaling in CCA cells resistant to EGFR inhibition by producing IGF2. **A,** Representative IHC staining of IGF1R and IGF2 in xenograft tumors from control and resistant CCA cells. White and black arrowheads indicate tumor cells and CAFs, respectively. Magnification, ×5 and ×40 (insets). **B,** Representative images of Western blot analysis of IGF2 expression in human liver–derived myofibroblasts cell lines (hTERT and LX2). **C,** Effect of erlotinib on the viability of control and resistant CCA cells. Cell viability was measured after 72 hours of incubation with the indicated compounds and/or medium (20 μmol/L erlotinib, 2 mg/mL IGF2-neutralizing antibody or an irrelevant IgG isotype, in the absence (white bars) or presence (black bars) of hTERT-HSC conditioned medium). The dotted line (vehicle) indicates the viability of the cells cultured in the absence of erlotinib. **D,** Representative images of Western blot analysis of IR and IGF1R total expression and phosphorylation state in EGI-1 control and resistant cells treated or not with hTERT-HSC–conditioned medium. **E,** Effect of erlotinib on the viability of control and resistant CCA cells. Cell viability was measured after 72 hours of incubation with the indicated compounds (20 μmol/L erlotinib, 2 mg/mL IGF2-neutralizing antibody or an irrelevant IgG isotype, in the absence (white bars) or presence (black bars) of 100 ng/mL IGF2). **F,** Representative images of Western blot analysis of IR and IGF1R total expression and phosphorylation state in EGI-1 control and resistant cells treated or not with IGF2. Values are expressed as means ± SEM from at least 3 independent cultures. *, $P < 0.05$; **, $P < 0.01$; ***, $P < 0.001$, comparing cells treated with IGF2 with untreated cells. †, $P < 0.05$; ††, $P < 0.01$; †††, $P < 0.001$, comparing cells treated with IGF2-neutralizing antibody with untreated cells of each group.

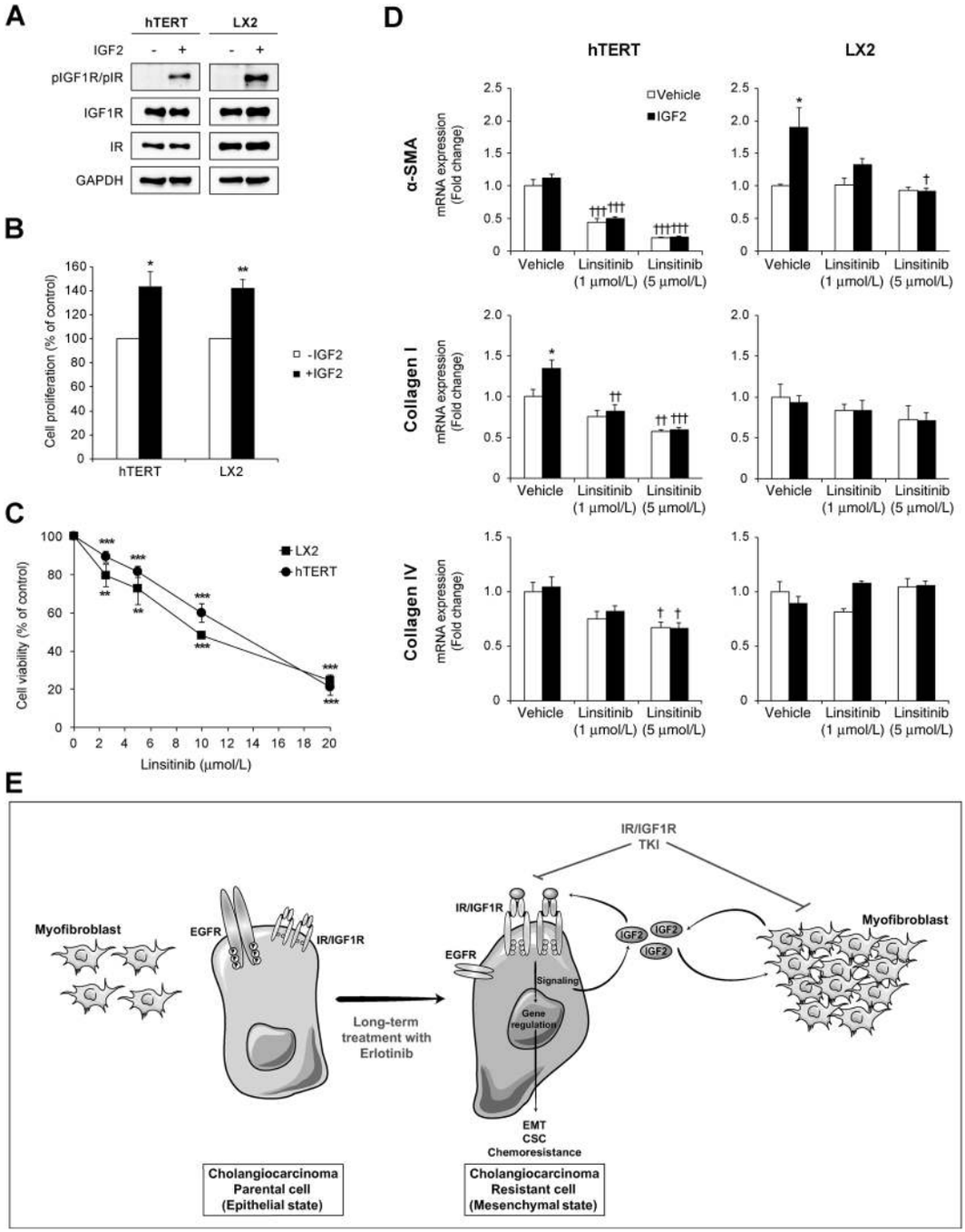

Figure 7.

IGF2/IR/IGF1R signaling regulates proliferation and activation of hepatic myofibroblasts. **A,** Representative images of Western blot analysis of IR and IGF1R total expression and phosphorylation state in hTERT-HSC and LX2 myofibroblastic cells. **B** and **C,** Effect of 100 ng/mL IGF2 (**B**) and linsitinib (**C**) on the proliferation of hTERT-HSC and LX2 cells. Cell viability was measured after 72 hours of incubation with IGF2 (in 0% FBS) or the indicated concentrations of linsitinib (in 10% FBS). **D,** mRNA expression analysis by RT-qPCR of α-SMA, collagens I and IV in hTERT-HSC, and LX2 cells. Cells were incubated for 48 hours with the indicated concentrations of linsitinib in the absence (white bars) or presence (black bars) of 100 ng/mL IGF2. **E,** Model depicting the adaptive mechanisms of CCA to EGFR inhibition. Chronic treatment with an EGFR inhibitor, erlotinib, promotes the overexpression of IGF2, IR, and IGF1R in CCA cells. IGF2/IR/IGF1R overexpression leads to the induction of a mesenchymal state in erlotinib-resistant CCA cells characterized by the adoption of EMT/CSC traits and chemoresistance. Resistant CCA cells to EGFR inhibition promote CAFs proliferation by unknown mechanisms. In the tumor microenvironment, CAFs produce IGF2 that contributes to chemoresistance of CCA cells by a paracrine loop. Thus, addition of IR/IGF1R inhibitor linsitinib reverses chemoresistance by acting on tumor cells and on CAFs proliferation/activation. CAFs, cancer-associated fibroblasts; CCA, cholangiocarcinoma; TKI, tyrosine kinase inhibitor. Values are expressed as means ± SEM from at least 3 independent cultures. *, $P < 0.05$; **, $P < 0.01$; ***, $P < 0.001$, comparing cells treated with IGF2 with untreated cells. †, $P < 0.05$; ††, $P < 0.01$; †††, $P < 0.001$, comparing cells treated with linsitinib with cells incubated with vehicle of each group.

(Fig. 7C). Similarly, IGF2 siRNA knockdown reduced hTERT-HSC proliferation (Supplementary Fig. S8A). Furthermore, the IGF2/IR/IGF1R pathway was able to regulate myofibroblast activation and collagen synthesis. IGF2 induced the expression of α-SMA in LX2 cells, which was abolished upon the addition of linsitinib (Fig. 7D). In contrast, the addition of exogenous IGF2 or inhibition of endogenous IGF2 by siRNA had no effect on α-SMA expression in hTERT-HSC cells, but again linsitinib was able to strongly inhibit the basal mRNA levels of α-SMA (Fig. 7D; Supplementary Fig. S8B). Regarding collagen synthesis, IGF2 induced the expression of collagen I and had no effect on collagen IV synthesis in hTERT-HSC cells. Linsitinib, but not IGF2 knockdown, reduced the expression of both collagens (Fig. 7D; Supplementary Fig. S8B). Contrarily, there was no visible effect of IGF2 or linsitinib on the expression of collagen variants in LX2 cells (Fig. 7D).

These observations provide further evidence of the role of the IGF2/IR/IGF1R signaling pathway on the regulation of stromal myofibroblasts biology and the therapeutic potential of linsitinib on these cells.

Discussion

Treatment of CCA patients remains challenging despite the identification of molecular pathways with high therapeutic potential such as EGFR (5–7, 27). Although antibodies or TKI against EGFR have shown efficacy in preclinical studies (27–29), they did not provide significant improvement of global survival in clinical trials in CCA (9–14). Here, we highlight resistance mechanisms whereby CCA cells evade EGFR inhibition. These include the adoption of EMT/CSC features that are regulated by the IGF2/IR/IGF1R signaling axis. In addition, we uncover a role of stromal CAFs on boosting IR/IGF1R signaling by producing IGF2 that could impair responsiveness to EGFR inhibition. Finally, we provide evidence that inhibition of IR/IGF1R combined with anti-EGFR in a preclinical model overcomes erlotinib resistance in CCA cells (Fig. 7E).

EMT is a developmental program strongly regulated by EMT-TF that allows cells to acquire mesenchymal properties at the expense of their epithelial characters conferring invasiveness and drug resistance capacities (20). We show a phenotypic switch from an epithelial to a mesenchymal phenotype in CCA cells subjected to chronic EGFR inhibition. The EMT-undergoing cells express higher levels of EMT-TF and mesenchymal markers, lower levels of E-cadherin compared with untreated cells, and display increased cell migratory capacity. Previous reports have shown a direct contribution of EMT-TF to the resistance to EGFR TKI in cancer (30, 31). In addition, we cannot exclude other described actions of EMT-TF, including upregulation of survival and anti-apoptotic signals rendering the cells less responsive to treatment (32). Moreover, a link between EMT and CSC generation and maintenance has been established in cancer (33). Indeed, cells presenting both EMT and CSC characteristics have been described in a malignant context (21). More specifically, EMT-TFs have been directly related to the induction of stemness by several mechanisms (21, 34, 35). Furthermore, EMT and CSC phenotypes have been shown to be regulated by the IGF signaling axis (24), a pathway that we found upregulated in erlotinib-resistant CCA cells. Interestingly, the specific molecular alterations among the four CCA cell lines were different regarding the upregulation of EMT-TF, mesenchymal, and CSC markers. Accordingly, GSEA showed enrichment in signatures associated with metastasis and stemness that were specific for erlotinib-resistant cells derived from each cell line. These differences are most probably accounted for the high heterogeneity of CCA (36, 37). Nevertheless, in spite of these molecular differences, the four CCA-resistant cell lines, with different origins along the biliary tree (i.e., intrahepatic or extrahepatic CCA), behaved phenotypically and, more importantly, functionally, in a similar way, by displaying higher migratory and tumorigenic properties, both under the regulation of an IGF2/IR/IGF1R signaling pathway.

A surprising fact is that, despite the rising interest of targeting EGFR in CCA and the increasing number of clinical trials testing different types of anti-EGFR therapies (i.e., erlotinib, lapatinib, cetuximab, and panitumumab), so far few studies have dedicated efforts into the understanding of mechanisms involved in anti-EGFR therapy resistance (14, 29, 38). Here, we identified the IGF axis as an alternative activated pathway in erlotinib-resistant CCA cells, and more specifically an upregulation of IR and IGF1R associated with increased expression of IGF2. This signaling pathway, described here for the first time as an adaptive mechanism to EGFR inhibition in CCA, has been implicated in resistance to EGFR targeting agents in other cancers, including glioblastoma (39), hepatocellular carcinoma (40), pancreatic (41), lung (23), and colorectal cancers (42). While the role of IR is currently unknown in CCA cells, IGF1R is involved in cholangiocyte proliferation and its expression is associated with an aggressive phenotype (43, 44). Consistent with the role of IR/IGF1R in erlotinib resistance in CCA cells, blockage of these receptors with the dual TKI linsitinib overcame erlotinib resistance and decreased EMT/CSC features. Interestingly, the involvement of IGF signaling axis in resistance to anti-EGFR has been shown in other tumors in response to not only erlotinib (23) but also lapatinib (45) and cetuximab (46). Thus, we could speculate that the IGF2/IR/IGF1R signaling pathway may play a more prominent role in the adaptive response to anti-EGFR therapy in CCA.

The tumor microenvironment plays a role not only in cancer progression but also in therapeutic response (47). In addition, cetuximab has been shown to induce CAFs activation in head and neck cancer patients, although whether these effects are mediated by directly acting on CAFs or indirectly through interactions with tumor cells is still unknown (48). Here, we show that erlotinib-resistant CCA tumors exhibited a higher stromal component, i.e., α-SMA–positive cells, than control CCA tumors, suggesting an impact of resistant tumor cells on CAFs proliferation by yet unidentified mechanisms. More importantly, we identified CAFs as IGF2-producing cells in mice xenograft and human CCA tumors, in accordance with previous studies in non–small cell lung (49), colon (25), and pancreatic cancers (41). In this context, we uncovered a potential role for IGF2 in the CAFs-CCA cross-talk by increasing erlotinib resistance in tumor cells. Furthermore, we confirmed the function of IR/IGF1R as inductors of fibroblast proliferation, as previously described in hepatic stellate cells from fibrotic liver settings and CAFs from other cancers (25, 50). Consequently, IR/IGF1R blockage showed inhibitory effects not only on erlotinib-resistant CCA cells but also on the stromal content of CAFs in mouse CCA tumors. Interestingly, siRNA knockdown experiments revealed a role of IGF2 in fibroblast proliferation but not in their myofibroblastic phenotype, suggesting an IGF2-independent effect for IR/IGF1R in fibroblast activation. Perhaps IR/IGF1R

heterodimerization with other RTK, a well-described phenomenon (51), could have taken part in this process. Collectively, our results argue for a wider role of the IGF system in the cross-talk between cancer cells and CAFs in resistance to erlotinib in CCA.

Altogether, the upregulation of IGF signaling pathway in our preclinical models of erlotinib resistance, together with the fact that all protagonists of the IGF axis are expressed by both tumor cells and CAFs in human CCA, may revive the interest of using combinatorial therapies with anti-EGFR together with anti-IR/IGF1R inhibitors as potential treatment for CCA patients.

Disclosure of Potential Conflicts of Interest

No potential conflicts of interest were disclosed.

Authors' Contributions

Conception and design: J. Vaquero, A. Clapéron, L. Fouassier
Development of methodology: J. Vaquero, C. Lobe, S. Tahraoui, M. Mergey, F. Merabtene, L. Fouassier
Acquisition of data (provided animals, acquired and managed patients, provided facilities, etc.): J. Vaquero, C. Lobe, D. Wendum L. Fouassier
Analysis and interpretation of data (e.g., statistical analysis, biostatistics, computational analysis): J. Vaquero, C. Lobe, D. Wendum, C. Coulouarn, C. Desbois-Mouthon, F. Praz, L. Fouassier
Writing, review, and/or revision of the manuscript: J. Vaquero, A. Clapéron, D. Wendum, C. Coulouarn, C. Housset, C. Desbois-Mouthon, F. Praz, L. Fouassier
Administrative, technical, or material support (i.e., reporting or organizing data, constructing databases): S. Tahraoui, M. Mergey, F. Merabtene, C. Housset, L. Fouassier
Study supervision: J. Vaquero, L. Fouassier

Acknowledgments

We acknowledge Wassila Carpentier from Sorbonne Université, Inserm, UMS Omique, Plateforme Post-génomique de la Pitié-Salpêtrière (P3S), Nicolas Cagnard, Plateforme Bio-informatique Paris Descartes, Hôpital Necker, Tatiana Ledent from Housing and experimental animal facility (HEAF), Centre de recherche Saint-Antoine (CRSA), Annie Munier and Romain Morichon from the Flow cytometry-imaging platform UMS_30 LUMIC, CRSA, and Claire Calmel from CRSA for help in genotyping CCA cells. We also thank Ester Gonzalez-Sanchez and Ander Arbelaiz for technical assistance and discussion of the manuscript, and Yves Le Bouc, Laurence Perin, and Patricia Leneuve for their advice on IGF2 protein detection.

L. Fouassier is supported by grants from Fondation de France (No. 2011 25574 and 2014 47502), La Ligue Nationale contre le Cancer (No. RS14/75-112), GEFLUC (2013), and ANR (ANR-17-CE14-0013-01. J. Vaquero is a recipient of the following postdoctoral fellowships from the Spanish Association for the Study of the Liver (AEEH), the Fondation ARC (No. PDF2014601431) and the LABEX PLAS@PAR (reference ANR-11-IDEX-0004-02). C. Lobe is recipient of a fellowship from la Ligue Nationale contre le Cancer (No.13014).

The costs of publication of this article were defrayed in part by the payment of page charges. This article must therefore be hereby marked *advertisement* in accordance with 18 U.S.C. Section 1734 solely to indicate this fact.

Received December 14, 2017; revised April 3, 2018; accepted April 27, 2018; published first May 1, 2018.

References

1. Banales JM, Cardinale V, Carpino G, Marzioni M, Andersen JB, Invernizzi P, et al. Expert consensus document: cholangiocarcinoma: current knowledge and future perspectives consensus statement from the European Network for the Study of Cholangiocarcinoma (ENS-CCA). Nat Rev Gastroenterol Hepatol 2016;13:261–80.
2. Marin JJG, Lozano E, Herraez E, Asensio M, Di Giacomo S, Romero MR, et al. Chemoresistance and chemosensitization in cholangiocarcinoma. Biochim Biophys Acta 2018;1864:1444–53.
3. Valle J, Wasan H, Palmer DH, Cunningham D, Anthoney A, Maraveyas A, et al. Cisplatin plus gemcitabine versus gemcitabine for biliary tract cancer. N Engl J Med 2010;362:1273–81.
4. Andersen JB, Spee B, Blechacz BR, Avital I, Komuta M, Barbour A, et al. Genomic and genetic characterization of cholangiocarcinoma identifies therapeutic targets for tyrosine kinase inhibitors. Gastroenterology 2012;142:1021–31e15.
5. Claperon A, Mergey M, Nguyen Ho-Bouldoires TH, Vignjevic D, Wendum D, Chretien Y, et al. EGF/EGFR axis contributes to the progression of cholangiocarcinoma through the induction of an epithelial-mesenchymal transition. J Hepatol 2014;61:325–32.
6. Yoon JH, Gwak GY, Lee HS, Bronk SF, Werneburg NW, Gores GJ. Enhanced epidermal growth factor receptor activation in human cholangiocarcinoma cells. J Hepatol 2004;41:808–14.
7. Sia D, Hoshida Y, Villanueva A, Roayaie S, Ferrer J, Tabak B, et al. Integrative molecular analysis of intrahepatic cholangiocarcinoma reveals 2 classes that have different outcomes. Gastroenterology 2013;144:829–40.
8. Yoshikawa D, Ojima H, Iwasaki M, Hiraoka N, Kosuge T, Kasai S, et al. Clinicopathological and prognostic significance of EGFR, VEGF, and HER2 expression in cholangiocarcinoma. Br J Cancer 2008;98:418–25.
9. Chen JS, Hsu C, Chiang NJ, Tsai CS, Tsou HH, Huang SF, et al. A KRAS mutation status-stratified randomized phase II trial of gemcitabine and oxaliplatin alone or in combination with cetuximab in advanced biliary tract cancer. Ann Oncol 2015;26:943–9.
10. Gruenberger B, Schueller J, Heubrandtner U, Wrba F, Tamandl D, Kaczirek K, et al. Cetuximab, gemcitabine, and oxaliplatin in patients with unresectable advanced or metastatic biliary tract cancer: a phase 2 study. Lancet Oncol 2010;11:1142–8.
11. Lee J, Park SH, Chang HM, Kim JS, Choi HJ, Lee MA, et al. Gemcitabine and oxaliplatin with or without erlotinib in advanced biliary-tract cancer: a multicentre, open-label, randomised, phase 3 study. Lancet Oncol 2012;13:181–8.
12. Leone F, Marino D, Cereda S, Filippi R, Belli C, Spadi R, et al. Panitumumab in combination with gemcitabine and oxaliplatin does not prolong survival in wild-type KRAS advanced biliary tract cancer: A randomized phase 2 trial (Vecti-BIL study). Cancer 2016;122:574–81.
13. Malka D, Cervera P, Foulon S, Trarbach T, de la Fouchardiere C, Boucher E, et al. Gemcitabine and oxaliplatin with or without cetuximab in advanced biliary-tract cancer (BINGO): a randomised, open-label, non-comparative phase 2 trial. Lancet Oncol 2014;15:819–28.
14. Pellat A, Vaquero J, Fouassier L. Role of ErbB/HER family of receptor tyrosine kinases in cholangiocyte biology. Hepatology 2017doi 10.1002/hep.29350.
15. Brivio S, Cadamuro M, Strazzabosco M, Fabris L. Tumor reactive stroma in cholangiocarcinoma: the fuel behind cancer aggressiveness. World J Hepatol 2017;9:455–68.
16. Choe C, Shin YS, Kim C, Choi SJ, Lee J, Kim SY, et al. Crosstalk with cancer-associated fibroblasts induces resistance of non-small cell lung cancer cells to epidermal growth factor receptor tyrosine kinase inhibition. Onco Targets Ther 2015;8:3665–78.
17. Johansson AC, Ansell A, Jerhammar F, Lindh MB, Grenman R, Munck-Wikland E, et al. Cancer-associated fibroblasts induce matrix metalloproteinase-mediated cetuximab resistance in head and neck squamous cell carcinoma cells. Mol Cancer Res 2012;10:1158–68.
18. Allain C, Angenard G, Clement B, Coulouarn C. Integrative genomic analysis identifies the core transcriptional hallmarks of human hepatocellular carcinoma. Cancer Res 2016;76:6374–81.
19. Chettouh H, Fartoux L, Aoudjehane L, Wendum D, Claperon A, Chretien Y, et al. Mitogenic insulin receptor-A is overexpressed in human hepatocellular carcinoma due to EGFR-mediated dysregulation of RNA splicing factors. Cancer Res 2013;73:3974–86.

20. Thiery JP, Acloque H, Huang RY, Nieto MA. Epithelial-mesenchymal transitions in development and disease. Cell 2009;139:871–90.
21. Mani SA, Guo W, Liao MJ, Eaton EN, Ayyanan A, Zhou AY, et al. The epithelial-mesenchymal transition generates cells with properties of stem cells. Cell 2008;133:704–15.
22. Fong JT, Jacobs RJ, Moravec DN, Uppada SB, Botting GM, Nlend M, et al. Alternative signaling pathways as potential therapeutic targets for overcoming EGFR and c-Met inhibitor resistance in non-small cell lung cancer. PLoS One 2013;8:e78398.
23. Suda K, Mizuuchi H, Sato K, Takemoto T, Iwasaki T, Mitsudomi T. The insulin-like growth factor 1 receptor causes acquired resistance to erlotinib in lung cancer cells with the wild-type epidermal growth factor receptor. Int J Cancer 2014;135:1002–6.
24. Malaguarnera R, Belfiore A. The emerging role of insulin and insulin-like growth factor signaling in cancer stem cells. Front Endocrinol (Lausanne) 2014;5:10.
25. Unger C, Kramer N, Unterleuthner D, Scherzer M, Burian A, Rudisch A, et al. Stromal-derived IGF2 promotes colon cancer progression via paracrine and autocrine mechanisms. Oncogene 2017;36:5341–55.
26. Cadamuro M, Stecca T, Brivio S, Mariotti V, Fiorotto R, Spirli C, et al. The deleterious interplay between tumor epithelia and stroma in cholangiocarcinoma. Biochim Biophys Acta 2018;1864:1435–43.
27. Pignochino Y, Sarotto I, Peraldo-Neia C, Penachioni JY, Cavalloni G, Migliardi G, et al. Targeting EGFR/HER2 pathways enhances the antiproliferative effect of gemcitabine in biliary tract and gallbladder carcinomas. BMC Cancer 2010;10:631.
28. Herberger B, Berger W, Puhalla H, Schmid K, Novak S, Brandstetter A, et al. Simultaneous blockade of the epidermal growth factor receptor/mammalian target of rapamycin pathway by epidermal growth factor receptor inhibitors and rapamycin results in reduced cell growth and survival in biliary tract cancer cells. Mol Cancer Ther 2009;8:1547–56.
29. Jimeno A, Rubio-Viqueira B, Amador ML, Oppenheimer D, Bouraoud N, Kulesza P, et al. Epidermal growth factor receptor dynamics influences response to epidermal growth factor receptor targeted agents. Cancer Res 2005;65:3003–10.
30. Yoshida T, Song L, Bai Y, Kinose F, Li J, Ohaegbulam KC, et al. ZEB1 mediates acquired resistance to the epidermal growth factor receptor-tyrosine kinase inhibitors in non-small cell lung cancer. PLoS One 2016;11:e0147344.
31. Chang TH, Tsai MF, Su KY, Wu SG, Huang CP, Yu SL, et al. Slug confers resistance to the epidermal growth factor receptor tyrosine kinase inhibitor. Am J Respir Crit Care Med 2011;183:1071–9.
32. Tiwari N, Gheldof A, Tatari M, Christofori G. EMT as the ultimate survival mechanism of cancer cells. Semin Cancer Biol 2012;22:194–207.
33. Fabregat I, Malfettone A, Soukupova J. New insights into the crossroads between EMT and stemness in the context of cancer. J Clin Med 2016;5. pii: E37. doi: 10.3390/jcm5030037.
34. Preca BT, Bajdak K, Mock K, Sundararajan V, Pfannstiel J, Maurer J, et al. A self-enforcing CD44s/ZEB1 feedback loop maintains EMT and stemness properties in cancer cells. Int J Cancer 2015;137:2566–77.
35. Tang B, Qi G, Tang F, Yuan S, Wang Z, Liang X, et al. Aberrant JMJD3 expression upregulates slug to promote migration, invasion, and stem cell-like behaviors in hepatocellular carcinoma. Cancer Res 2016;76:6520–32.
36. Brandi G, Farioli A, Astolfi A, Biasco G, Tavolari S. Genetic heterogeneity in cholangiocarcinoma: a major challenge for targeted therapies. Oncotarget 2015;6:14744–53.
37. Komuta M, Govaere O, Vandecaveye V, Akiba J, Van Steenbergen W, Verslype C, et al. Histological diversity in cholangiocellular carcinoma reflects the different cholangiocyte phenotypes. Hepatology 2012;55:1876–88.
38. Jimeno A, Kulesza P, Kincaid E, Bouaroud N, Chan A, Forastiere A, et al. C-fos assessment as a marker of anti-epidermal growth factor receptor effect. Cancer Res 2006;66:2385–90.
39. Ma Y, Tang N, Thompson RC, Mobley BC, Clark SW, Sarkaria JN, et al. InsR/IGF1R pathway mediates resistance to EGFR inhibitors in glioblastoma. Clin Cancer Res 2016;22:1767–76.
40. Desbois-Mouthon C, Cacheux W, Blivet-Van Eggelpoel MJ, Barbu V, Fartoux L, Poupon R, et al. Impact of IGF-1R/EGFR cross-talks on hepatoma cell sensitivity to gefitinib. Int J Cancer 2006;119:2557–66.
41. Ireland L, Santos A, Ahmed MS, Rainer C, Nielsen SR, Quaranta V, et al. Chemoresistance in pancreatic cancer is driven by stroma-derived insulin-like growth factors. Cancer Res 2016;76:6851–63.
42. Vigneri PG, Tirro E, Pennisi MS, Massimino M, Stella S, Romano C, et al. The insulin/IGF system in colorectal cancer development and resistance to therapy. Front Oncol 2015;5:230.
43. Alvaro D, Barbaro B, Franchitto A, Onori P, Glaser SS, Alpini G, et al. Estrogens and insulin-like growth factor 1 modulate neoplastic cell growth in human cholangiocarcinoma. Am J Pathol 2006;169:877–88.
44. Ohashi H, Adachi Y, Yamamoto H, Taniguchi H, Nosho K, Suzuki H, et al. Insulin-like growth factor receptor expression is associated with aggressive phenotypes and has therapeutic activity in biliary tract cancers. Cancer Sci 2012;103:252–61.
45. Corcoran C, Rani S, Breslin S, Gogarty M, Ghobrial IM, Crown J, et al. miR-630 targets IGF1R to regulate response to HER-targeting drugs and overall cancer cell progression in HER2 over-expressing breast cancer. Mol Cancer 2014;13:71.
46. Li X, Xu L, Li H, Zhao L, Luo Y, Zhu Z, et al. Cetuximab-induced insulin-like growth factor receptor I activation mediates cetuximab resistance in gastric cancer cells. Mol Med Rep 2015;11:4547–54.
47. Cadamuro M, Brivio S, Spirli C, Joplin RE, Strazzabosco M, Fabris L. Autocrine and paracrine mechanisms promoting chemoresistance in cholangiocarcinoma. Int J Mol Sci 2017;18. pii: E149. doi: 10.3390/ijms18010149.
48. Schmitz S, Bindea G, Albu RI, Mlecnik B, Machiels JP. Cetuximab promotes epithelial to mesenchymal transition and cancer associated fibroblasts in patients with head and neck cancer. Oncotarget 2015;6:34288–99.
49. Chen WJ, Ho CC, Chang YL, Chen HY, Lin CA, Ling TY, et al. Cancer-associated fibroblasts regulate the plasticity of lung cancer stemness via paracrine signalling. Nat Commun 2014;5:3472.
50. Svegliati-Baroni G, Ridolfi F, Di Sario A, Casini A, Marucci L, Gaggiotti G, et al. Insulin and insulin-like growth factor-1 stimulate proliferation and type I collagen accumulation by human hepatic stellate cells: differential effects on signal transduction pathways. Hepatology 1999;29:1743–51.
51. Liefers-Visser JAL, Meijering RAM, Reyners AKL, van der Zee AGJ, de Jong S. IGF system targeted therapy: therapeutic opportunities for ovarian cancer. Cancer Treat Rev 2017;60:90–9.